Optics and Lasers in Engineering 50 (2012) 359–365

Contents lists available at SciVerse ScienceDirect

Optics and Lasers in Engineering

journal homepage: www.elsevier.com/locate/optlaseng

Effects of the induced birefringence in photorefractive crystals on speckle optical vortices

Jorge A. Gómez [a,b,*], Edgar Rueda [c], Ángel Salazar [a], Myriam Tebaldi [d], Nestor Bolognini [d,e], Alberto Lencina [d,e]

[a] Grupo de Óptica y Espectroscopía (GOE), Centro de Ciencia Básica, Universidad Pontificia Bolivariana, A.A. 56006 Medellín, Colombia
[b] Grupo de Física Básica y Aplicada, Politécnico Colombiano Jaime Isaza Cadavid, Medellín, Colombia
[c] Grupo de Óptica y Fotónica, Instituto de Física, Universidad de Antioquia, A.A 1226 Medellín, Colombia
[d] Centro de Investigaciones Ópticas (CONICET La Plata-CIC) and UID OPTIMO, Facultad de Ingenieria, Universidad Nacional de La Plata, P.O. Box 3 C.P 1897, La Plata, Argentina
[e] Departamento de Física, Facultad de Ciencias Exactas, Universidad Nacional de La Plata, Argentina

ARTICLE INFO

Article history:
Received 30 August 2011
Received in revised form
28 October 2011
Accepted 31 October 2011
Available online 21 November 2011

Keywords:
Optical vortices
Speckle
Photorefractive

ABSTRACT

In this work, we show that it is possible to change the properties of an optical vortex formed in a speckle pattern by the control of an external electric field applied to a sillenite-type photorefractive material in a non-holographic configuration. To show it, a scheme that allows the recovering of both, the polarization state and the phase distribution of an optical field was implemented. Changes in the polarization state of the light in the neighborhood of the vortex were observed with the application of an external electric field. Likewise, changes in the phase structure around the vortex and displacements of the vortices themselves were measured. These displacements have a fairly linear dependence on the applied field to the photorefractive crystal. Experimental results are qualitatively explained with the theoretical treatment of non-holographic recording in photorefractive crystals.

1. Introduction

It is well known that speckles appear when a diffusing surface is illuminated by coherent light. The speckle patterns have interesting and important applications in metrology and image processing [1,2]. Displacements, tilts, and deformations of the input diffuser produce displacements and structural changes in the speckle patterns, which can be analyzed on the basis of the correlation operations [3–5]. Recently, other particularities of the speckle patterns have been proposed in a wide range of engineering applications [6–8].

A fully developed speckle can be understood as an optical noise with a negative exponential probability density function whose maximum value is located at zero intensity. Statistically, the probability of occurrence of absolute zero intensity in a point into a speckle distribution is zero. However, even so, points with zero intensity can occur [1]. These points are known as nodal points, phase singularities, wave dislocations, or optical vortices [6].

An optical vortex is a point with a phase indetermination, and around it, all values of the phase are present [9]. For this reason, the energy flows circularly in the same direction of the phase variation [10]. Optical vortices are usually characterized by their spin angular momentum (SAM), associated with the polarization state of the field, and their orbital angular momentum (OAM), associated with the spatial structure of the field and the phase [11,12]. Techniques of spin–orbital exchange have been demonstrated with inhomogeneous birefringence devices [13]. Many experimental and theoretical studies have been performed on optical vortices in speckle patterns [14–18]. Unlike the optical vortices in Laguerre-Gaussian beams, the vortices in speckle patterns are anisotropic. It means that the phase of the field does not increase linearly with the azimuthal angle around the singularity [19,20]. On the other hand, in speckle patterns, the phase singularities almost perfectly compensate each other, so the net topological charge of the speckle pattern is very close to zero. This balance is due to coexistence of vortex–antivortex pairs [21]. The phase singularities inside each vortex–antivortex pair move around each other and rope-like structures are formed in free space propagation [22]. The phase singularities in a speckle pattern may be experimentally detected by the interference of the speckle pattern with a plane wave. The position of the vortex coincides with the position of a fork-like structure in the interference pattern [14].

One of the most important applications of the optical vortices is the optical tweezers [23]. In this kind of arrangement, colloidal particles are trapped into the vortex. Speckle fields have shown to be suitable for trapping nanometer objects and cooling atoms [24–26]. Recently, in Ref. [27], it demonstrated the possibility of using 3D clustered speckle pattern in an optical tweezer setup. Likewise, the use of volume speckle in trapping has been recently

* Corresponding author at: Grupo de Física Básica y Aplicada. Politécnico Colombiano Jaime Isaza Cadavid, Medellín, Colombia.
E-mail address: jagomez@elpoli.edu.co (J.A. Gómez).

0143-8166/$ - see front matter © 2011 Elsevier Ltd. All rights reserved.
doi:10.1016/j.optlaseng.2011.10.021

reported [28]. In any trapping arrangement, it is important to implement ways to change the dynamics condition of the particles and, when optical vortices are used, the modification of the angular momentum is the way to reach it [13].

On the other hand, it is well known that photorefractive crystals have been widely used in dynamic holography, light amplification, optical conjugation, optical signal processing, sensing systems, and spatial light modulators [29–35]. These materials are well suited for such applications because of their ability to encode light intensity distributions by refractive index changes. In particular, the sillenite photorefractive crystals (BSO, BGO, BTO) are fast and sensitive materials adequate for real time procedures [36]. In non holographic arrangements, it is possible to demonstrate that when an external electric field is applied to the crystal, the induced birefringence, via electro–optic effect has its maximum in the dark regions and it is approximately zero in the more illuminated regions [37]. Here, it is important to highlight that, if a speckle pattern is imaged on a photorefractive crystal in non holographic scheme, when external electric field is applied to the crystal, in the points where optical vortex appears, the induced birefringence has a maximum, which can be very useful in the modification of the vortex characteristics.

In this work, an experimental methodology that allows evaluating the effect of the induced birefringence in a photorefractive material on speckle optical vortices is implemented. A speckle pattern generated by a diffuser element was registered in a BSO crystal in a non holographic configuration, and an electric field was applied to the photorefractive material. Maps of Stokes parameters and phase distributions were then obtained by two experiments using the same setup. Changes in the polarization state and in the phase of the optical field in the neighborhoods of the vortices were registered. Moreover, displacements of the phase singularities were detected and, a fairly linear dependence of the displacements on the external applied field was observed. Experimental results are qualitatively well explained using the simplified one dimensional model for birefringence recording in photorefractive materials. These observations can be of great utility in applications of speckle patterns in several engineering application and, particularly, in optical tweezers.

2. Theoretical and experimental analysis

In general, an optical speckle pattern can be mathematically expressed as a sum of random phasors as [1],

$$U = Ae^{j\theta} = \frac{1}{\sqrt{N}} \sum_{n=1}^{N} a_n e^{j\phi_n} \tag{1}$$

where N represents the number of components in the random walk, U represents the resultant phasor, A represents the amplitude of U and θ its phase; a_n and ϕ_n are the amplitude and phase of the *nth* component of a phasor in the sum. The random walk can be expressed in terms of their real and imaginary parts as,

$$\mathrm{Re}\{U\} = \frac{1}{\sqrt{N}} \sum_{n=1}^{N} a_n \cos\phi_n$$

$$\mathrm{Im}\{U\} = \frac{1}{\sqrt{N}} \sum_{n=1}^{N} a_n \sin\phi_n \tag{2}$$

Furthermore, if a_n and ϕ_n are statistically independent quantities for each optical phasor, if the phase distribution of ϕ_n is uniform on the interval $(-\pi, \pi)$, and if the number of phasors is large, the intensity probability density function has a negative exponential behavior, in this way:

$$p_I(I) = \frac{1}{\bar{I}} e^{-(I/\bar{I})}. \tag{3}$$

A speckle pattern with this statistical distribution is known as a fully developed speckle. In Fig. 1, a typical experimental speckle distribution generated by 532 nm laser radiation impinging in a diffuser, and its corresponding intensity histogram, are presented. Although from the Eq. (3), it is possible to conclude that the probability of occurrence of precisely zero intensity is null, in a speckle pattern this is an event that indeed does occur [1]. Zero intensity is obtained if both the real and imaginary parts of the field are zero at the same point of the speckle pattern. In this way, at the location of a zero of intensity, the phase is undefined, and around of such a point, the whole $(0, 2\pi)$ range of phases appears. This means that there is a net change of phase in a circuit C enclosing the zero intensity point, which is quantized in units of 2π, as

$$q = \frac{1}{2\pi} \oint_C \vec{\nabla}\theta \bullet d\vec{r} \tag{4}$$

The integer q, positive or negative, is called the topological charge of the singularity. The sign of q is positive if the phase increases in a right handed sense. For an optical field, the current, which is the Poynting vector of the electromagnetic field, takes the form [10],

$$.\vec{J} = \mathrm{Im}[.U^* \vec{\nabla} U] = A^2 \vec{\nabla}\theta \tag{5}$$

Because the vector $\vec{J}$ is in direction of the phase change, $\vec{\nabla}\theta$, the phase singularity is therefore the optical vortex of the optical current flow. In the Fig. 2, the 3D image of an optical speckle vortex reconstructed with our experimental set up, is presented.

On the other hand, it is well known that photorefractive crystals can exhibit induced birefringence via the linear electro–optic effect. Let us remember the physical mechanism by which optical information can be stored in a photorefractive material by

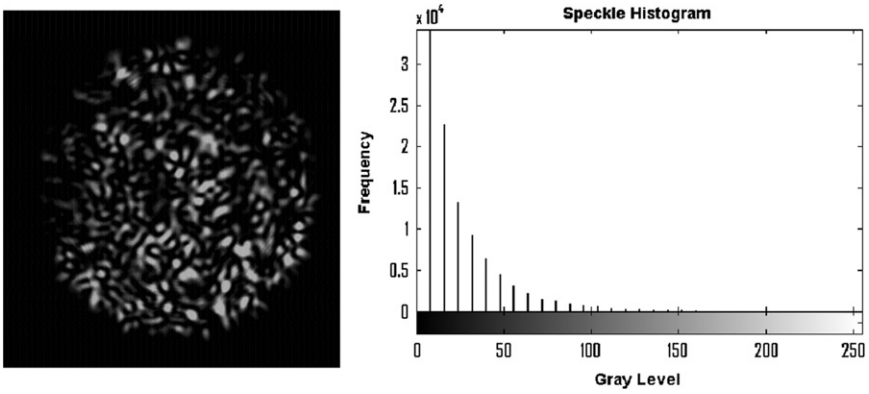

Fig. 1. Typical experimental fully developed speckle distribution and its intensity histogram.

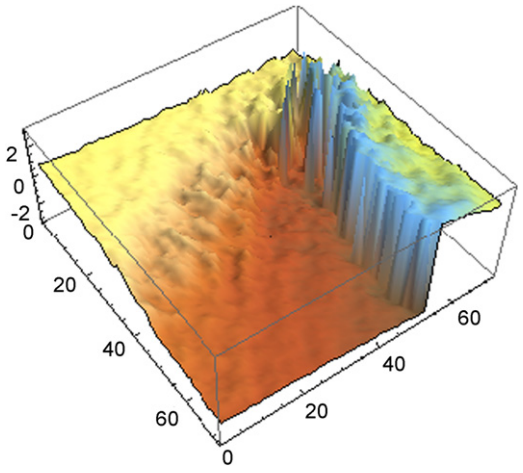

Fig. 2. Experimental speckle vortex.

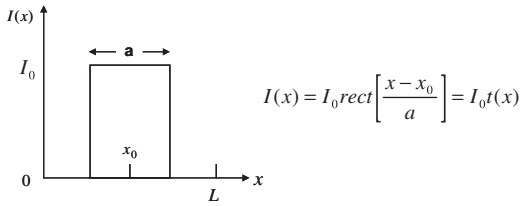

Fig. 3. Uniform rectangular light distribution.

a non holographic register. When a voltage V is applied to the crystal, with a distance L between electrodes, it becomes uniformly birefringent due to the external electric field $E_0 = V/L$. A light intensity distribution incident onto the crystal generates photo-charges that are drifted by the field E_0. A space charge field E_{SC} is created, which partially compensates the external field in the illuminated regions. In this way, if the light intensity distribution is not uniform, the resulting internal electric field $E = E_{SC} + E_0$ modifies locally the refraction index via Pockels effect.

In our experimental arrangement, the external electric field is orthogonal to the face (110) of a Bi12SiO20 (BSO) crystal and the light is incident on the face $(1\bar{1}0)$. Therefore, the induced birefringence modulation δn can be calculated as [38],

$$\delta n(x) = n_0^3 r_{41} E(x) \tag{6}$$

where r_{41} is the electro–optic coefficient and n_0 is the average refractive index at the writing wavelength.

It is possible to show, following the treatment in Ref. [39], that if the crystal is illuminated by an uniform rectangular pattern with a width a, as showed in the Fig. 3, and given by, $I_i(x) = I_0 t(x)$, where $I_i(x)$ is the light pattern onto the crystal, I_0 is the highest intensity value, and $t(x)$ is a normalized binary intensity distribution, the induced birefringence can be expressed as:

$$\delta n(x,V) = \begin{cases} \delta n = 0 & \text{if } t(x) = 1, \\ \delta n = n_0^3 r_{41} \frac{V}{L-a} & \text{if } t(x) = 0 \end{cases} \tag{7}$$

From Eq. (7), it is clear that, if we assume a speckle grain as a simple rectangular distribution of light, and having into account that the speckle size is shorter than the size of the crystal, the induced birefringence on the crystal just in the zone where the speckle is, can be written as $\delta n = n_0^3 r_{41}(V/L)$ for the surrounding dark regions, and zero in the illuminated zones. This is an interesting fact; because the vortices in the speckle pattern are in dark zones of the pattern, these appear to be located just in the regions where a maximum induced birefringence is obtained in the non-holographic recording scheme. In this way, it is possible to expect that when an electric field is applied to a photorefractive crystal, the field has a significant effect on the vortices of the pattern due to the local modification of the birefringence. Consequently, these effects have a direct implication on the angular momentum of the radiation.

To experimentally demonstrate these effects, let us consider the experimental setup of Fig. 4. In this scheme, a laser source of 532 nm and 150 MW of optical power is divided by the beam splitter B/S_1 to generate in a branch of the setup, a speckle field and, in another one, a plane wave to form a Mach–Zehnder interferometer. In our configuration, when the shutter SH is switched off, only the speckle pattern is registered by the analyzer system. When the shutter is open, the superposition of the plane wave and the speckle pattern is obtained. Using this experimental setup and the analyzer system formed by a first order quarter waveplate and a linear polarizer, it is possible to recover the Stokes parameters of the speckle field and its respective phase distribution. These procedures will be described below.

A subjective speckle pattern is formed by the diffuser, the lens L_1, and the aperture pupil AP with a diameter of 6 cm adjacent to the lens. A 1 cm × 1 cm × 1 cm BSO crystal is used to record the speckle pattern. Light is incident on the crystallographic plane $(1\bar{1}0)$ for a higher birefringence [36]. The optical activity of the crystal at 532 nm was previously measured as 36°/mm. A linear polarizer P_1 is located before the BSO crystal to guarantee horizontal polarization of the output beam in absence of an external electric beam. When an electric field is applied orthogonally to the face (110), the light emerges from the crystal elliptically polarized and the phase of the speckle pattern is also modified. In the observation plane, a magnifier optical system (5 ×) was inserted in front of the CCD camera. This system allows

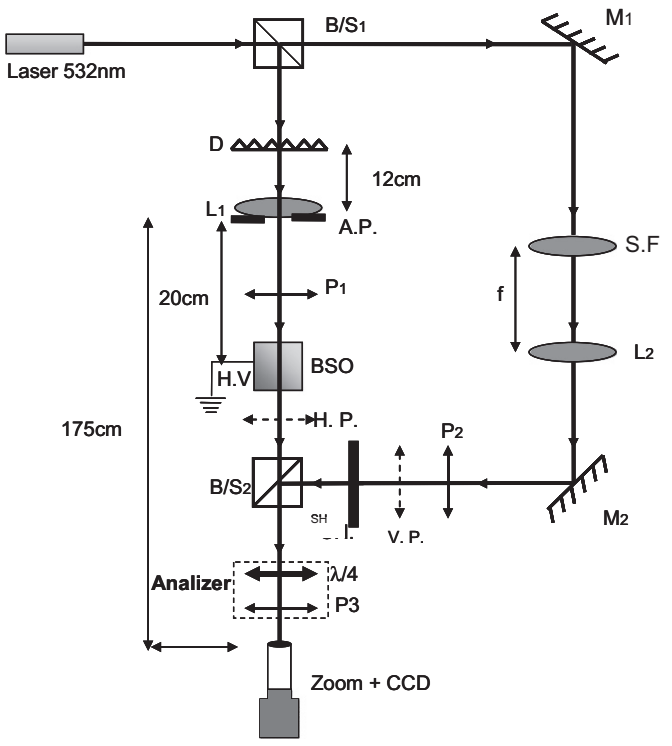

Fig. 4. Diagram of the experimental setup. B/S1 and B/S2: Beam splitters, D: Diffuser, M_1 and M_2: Mirrors, A.P.: Aperture pupil, $\lambda/4$: Rotating first order quarter-waveplate, P1 and P2: Fixed polarizers, P3: Rotating polarizer, S.F: Spatial filter, H.P.: Horizontal Polarization, V.P.: Vertical Polarization, L1 and L2: Lenses, SH: Shutter, BSO: 1 cm × 1 cm × 1 cm BSO crystal, H.V: High voltage source, Zoom + CCD: Magnification system and CCD high resolution camera.

evaluating the behavior of the speckle pattern in a few speckle grains.

In Fig. 5, images of the speckle patterns registered without magnification and with the maximum magnification ($5\times$) are presented. When the electric field is applied to the crystal, changes of the speckle pattern are observed at the detection plane. In Fig. 6, a section of the speckle pattern registered before and after applying a field of 6 kV/cm to the crystal is shown. In the same figure, a small region for both situations, framed in white lines, is zoomed. An evident distortion of the speckle pattern section is appreciated. It seems to be clear, that the significant changes in the speckle patterns occur in the regions with the lower intensity. On the contrary, the brighter regions are practically unmodified by the action of the electric field. This is in agreement with the birefringence model for non-holographic registers in the photorefractive material, as was mentioned before. This is an important observation because the optical vortices are present in completely dark regions. In Fig. 7, the normalized self-correlation [40] of the speckle pattern without external electric field and its cross-correlation for different values of the electric field are presented. From this figure, it is evident that the distortion of the speckle pattern depends on the intensity of the field, and the correlation decreases linearly as the field increases. To evaluate the effects of the induced birefringence on the polarization and phase of the speckle pattern, Stokes parameter maps and phase distributions were calculated.

The Stokes parameters allow describing completely the polarization state of polarized, unpolarized and partially polarized light beams. Considering the z direction along the crystal depth, the components of the optical field $E_x(z,t)$ and $E_y(z,t)$ are given by,

$$E_x(z,t) = E_{0x}\cos(wt-kz+\delta_x)$$
$$E_y(z,t) = E_{0y}\cos(wt-kz+\delta_y) \quad (8)$$

where t represents time, E_{0x} and E_{0y} are the maximum amplitudes of the optical field, w is the angular frequency, $k=2\pi/\lambda$ is the wave number, and δ_x and δ_y are phase constants. With these definitions, it is possible to define the Stokes parameters as,

$$S_0 = E_{0x}^2+E_{0y}^2; \quad S_1 = E_{0x}^2-E_{0y}^2;$$
$$S_2 = 2E_{0x}E_{0y}\cos\delta; \quad S_3 = 2E_{0x}E_{0y}sen\delta$$
$$\delta = \delta_x-\delta_y \quad (9)$$

In Eq. (9), the parameter S_0 describes the total intensity of the field, S_1 describes the preponderance of linearly horizontally polarized light over linearly vertically polarized light, S_2 describes the preponderance of linear $+45^\circ$ polarized light over linear -45° polarized light, and S_3 describes the preponderance of right circularly polarized light over left circularly polarized light. When the light is completely polarized, the relationship $S_0^2 = S_1^2+S_2^2+S_3^2$ is satisfied, and in the other cases $S_0^2 \le S_1^2+S_2^2+S_3^2$ [41].

As was mentioned, when the shutter in the experimental setup of the Fig. 5 is open, the Stokes parameters can be calculated. To recover the Stokes parameters an alternative methodology proposed in [42] was proved and improved. According to [42], the quarter-waveplate must be rotated in steps of θ° maintaining fixed polarizer. An analysis of this system shows that the intensity of the optical beam on the detector can be written in terms of the Stokes parameters as [41],

$$I(\theta) = \frac{1}{2}(S_0+S_1\cos^2(2\theta)+S_2\cos(2\theta)\sin(2\theta)+S_3\sin(2\theta)) \quad (10)$$

In Ref. [42] it is shown that Eq. (10) can be rewritten as a truncated Fourier series consisting of, a dc term, a second harmonic term and two fourth harmonic terms. In this paper, it is proposed that the Stokes parameters can be calculated with a minimum of eight data corresponding to the measured intensity for the same number of rotations of the quarter-waveplate. However, in our case, the suggested method was proved with eight and more data points without physical meaning for the result. But, taking advantage of the knowledge of the analytical expression for the intensity variation in Eq. (10), an algorithm of global minimization was implemented with the software Mathematica. The command NMinimize, which is based on the Nelder–Mead method [43], was restricted with the "constrained conditions" $0<S_0<1<$, and $-1<S_i<1$ for $i=1, 2, 3$. In this way, and with a calibration in the CCD camera, which allowed having linear behavior from 10 to 255 in a gray scale, was possible to construct in each pixel of the speckle pattern the set of data to recover the Stokes parameters. The estimated error in the method was around 5% and, in pixels where the intensity falls below 10 in the linear gray scale, the method had no good results. In Fig. 8, the experimental behavior of the intensity for linearly polarized speckle pattern in an arbitrary pixel and the numerical fitting to the experimental data are presented.

Due to the elevated computational cost of the calculus for the whole speckle pattern, the method for the determination of the Stokes parameters was ran in small regions where, by inspection eventually an optical vortex could exist because of its light distribution, i.e, regions where very dark points appear.

In Fig. 9, a map of the Stokes parameters is presented for the highlighted region in Fig. 6. In this map, because the evident change in the Stokes parameters, it is clear the modification of the polarization state of the speckle when a field of 6 kV/cm was applied. Here, it is important to appreciate that the higher changes are evident in the zones where the intensities are low, but not in the darker regions. It is due that the threshold of 10 Gy

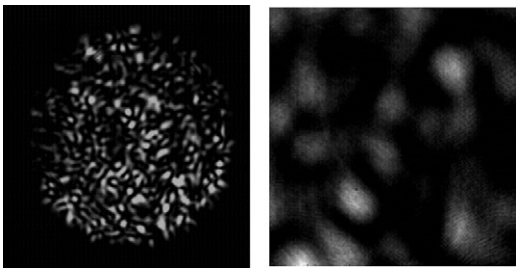

Fig. 5. Registered speckle patterns without magnification and with magnification $5\times$.

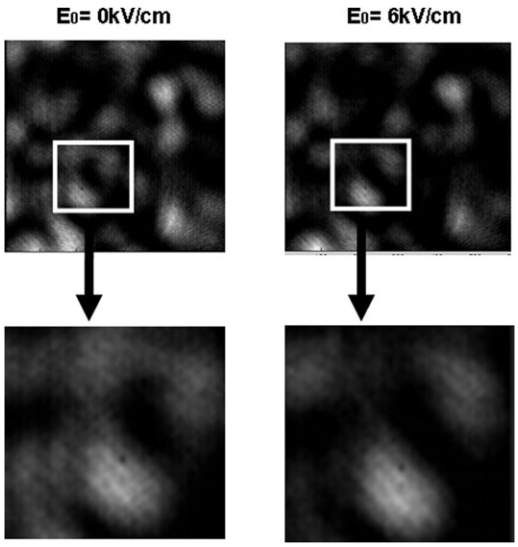

Fig. 6. Distortion of the speckle pattern when a 6 kV/cm field is applied to the BSO crystal.

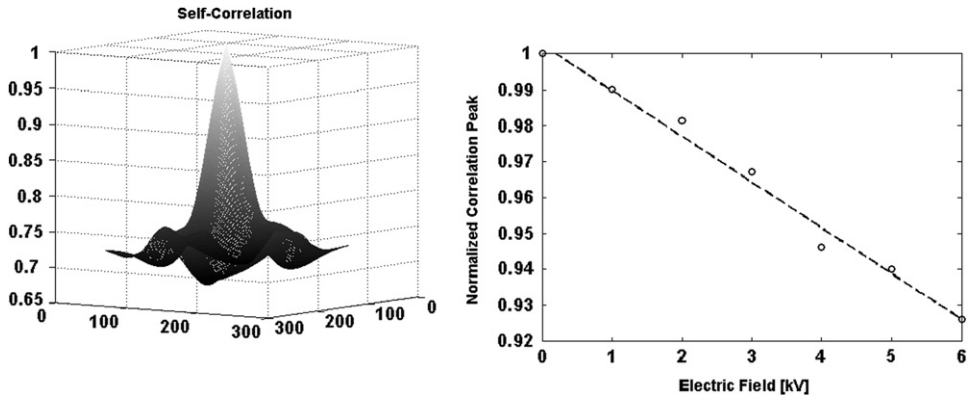

Fig. 7. Normalized self-correlation without external electric field and behavior of the correlation vs. applied electric field.

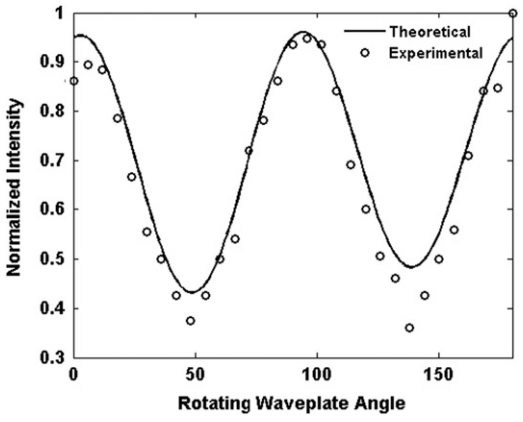

Fig. 8. Experimental data and numerical fitting for intensity vs. rotation angle of the quarter wave plate, in an arbitrary pixel.

levels in the calibration of the CCD camera does not allow to discriminate those points.

To analyze the effect of the induced birefringence on the regions where the Stokes parameters were not recovered, a reconstruction of the phase of the speckle pattern was realized. The phase of the speckle pattern was recovered by the method proposed by Denisenko et al. in [44]. In our experimental setup and, as was previously mentioned, when the shutter SH is open, the experimental conditions to recover the phase and its singularities are given. In this case, and according to the definitions in Eq. (9), when the Mach–Zehnder interferometer is formed, the CCD camera registers the superposition of the speckle pattern and a plane wave. In this way, the difference of phase between the two waves can be calculated as [44],

$$\delta = \tan^{-1}(S_3/S_2)$$
$$S_2 = I(45,45) - I(135,135)$$
$$S_3 = I(45,0) - I(135,0) \quad (11)$$

where $I(\alpha,\beta)$ is the intensity measured by the CCD when in the analyzer system of the Fig. 4, the polarizer and the quarter wave plate are rotated at angles α and β with respect to the horizontal direction, respectively. This definition of the Stokes parameters ensures cancellation of a common background in the intensity measurements, improving their accuracy significantly. In Fig. 10, the analyzed speckle pattern, its interferogram, and the phase distribution are presented. It is clear that, in regions where a fork shape is identified in the interferogram, a vortex is located in the phase map, as indicated by red circles. The location of the vortices by the phase reconstruction is convenient due to its independence on the width and the contrast of the fringes [44].

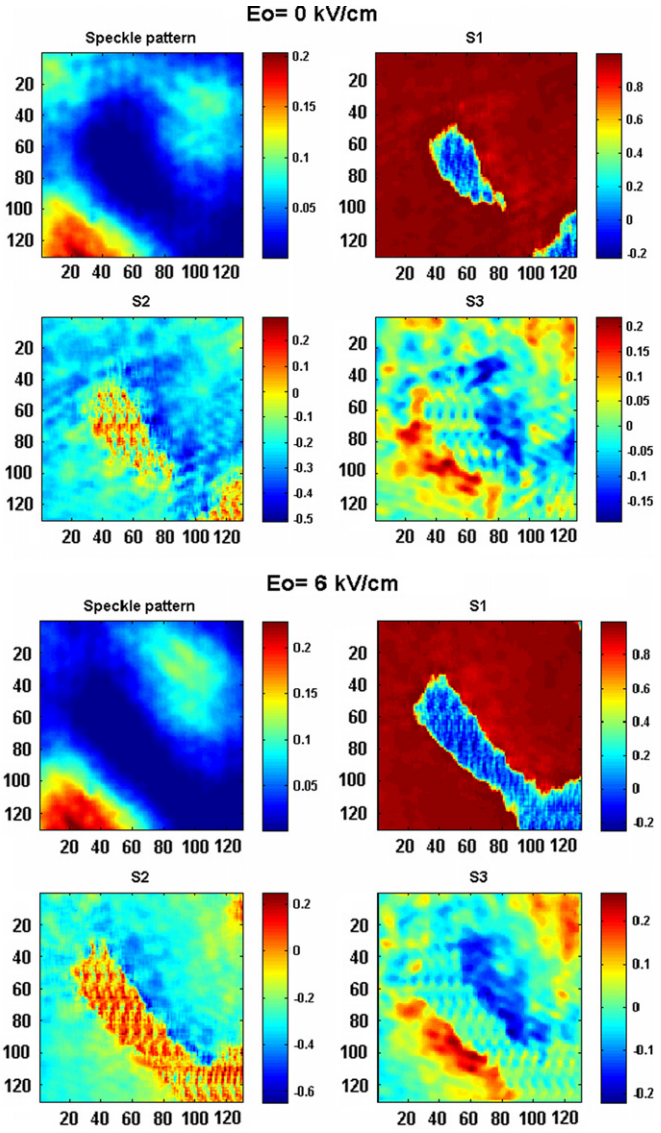

Fig. 9. Stokes parameters maps for a speckle pattern before and after applying an external electric field of 6 kV/cm to the crystal.

Phase maps were reconstructed for the speckle pattern when the BSO crystal was submitted to different values of the external electric field. Changes in the phase structure in the neighborhood of the vortices, and moreover, in its location were appreciated. In Fig. 11, the modification and displacement of a vortex due to the

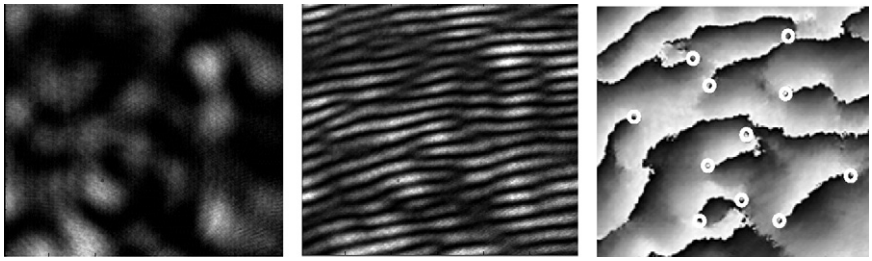

Fig. 10. Speckle pattern, interferogram and phase map. The white circles highlight optical vortices. (For interpretation of the references to colour in this figure legend, the reader is referred to the web version of this article.)

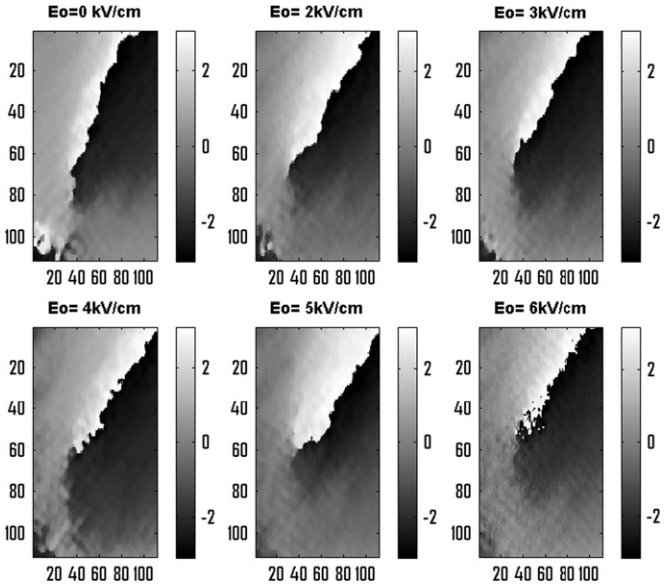

Fig. 11. Displacement of an optical vortex.

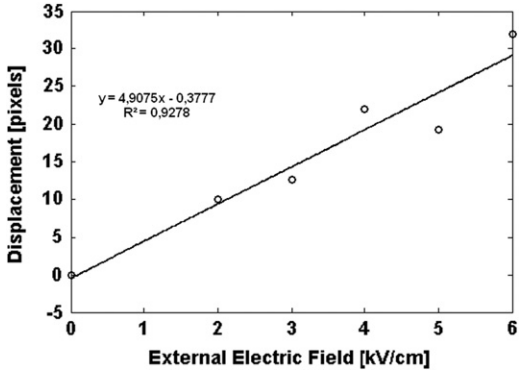

Fig. 12. Displacement of the optical vortices vs. applied field.

electrically controlled birefringence of the crystal is presented. The distance between the displaced vortex and the original vortex was calculated. For the estimation of the vortex displacement, the dependence of the speckle size, $\langle L_x \rangle = \lambda z/D$, was used. $\langle L_x \rangle$ is the average width of the speckle, z is the distance from the lens L1 to the crystal, λ is the illumination wavelength, and D is the diameter of the pupil aperture adjacent to the lens. In this way and, taking into account a pixel size of 4 μm, the estimated displacement in the CCD camera plane was 120 μm. It corresponds to a displacement of 13.3 μm in the inside crystal plane, approximately. As shown in Fig.12, a fairly linear behavior for the vortex displacement as a function of the applied electric field was found.

3. Conclusions

In this work, the possibility of changing the properties of an optical vortex produced in a speckle pattern by the control of the birefringence by an electric field applied to a photorefractive material in a non-holographic configuration was shown. Maps of Stokes parameters and phase were reconstructed by a technique that allowed recovering both quantities with the same analyzer system through polarimetric measures. Significant changes in the polarization state of the light in the neighborhood of the vortex were observed. Likewise, changes in the phase structure around the vortex, and displacements of the vortices were observed. The measured displacements showed a fairly linear dependence on the externally applied field to the photorefractive crystal. Experimental results were qualitatively well explained using the theoretical treatment of non-holographic recording in photorefractive crystals. These results here presented could be useful for applications concerning the control of the angular momentum of the radiation, and particularly in optical trapping.

Acknowledgments

J.A. Gómez acknowledges the financial support of the Politécnico Colombiano Jaime Isaza Cadavid for his Ph.D studies; of Colciencias for the resources to develop the doctoral stay in the Centro de Investigaciones Ópticas, CIOp, La Plata, Argentina and; special acknowledgments to the staff of the CIOp by their unconditional aids in this work. A. Salazar acknowledges to the CIDI of the Universidad Pontificia Bolivariana. E. Rueda acknowledges to the CODI of the Universidad de Antioquia. A. Lencina, M. Tebaldi, and N. Bolognini, acknowledge the financial support through CONICET no. 0863, ANCyT PICT 1167 and Facultad de Ingeniería, Universidad Nacional de La Plata no. 11/I125 (Argentina).

References

[1] Goodman JW. Speckle phenomena in optics. Roberts and Company; 2006.
[2] Rastogi P. Digital speckle pattern interferometry and related techniques. John Wiley and Sons; 2001.
[3] Majles Ara MH, Sirohi RS. Speckle interferometry methods for displacements and strain measurements using photorefractive crystals. Optik 2007;118: 445–51.
[4] Gasvik K. Optical Metrology. John Wiley and Sons; 2002.
[5] Tripathi R, Pati GS, Kumar A, Singh K. In-plane displacement measurement using a photorefractive speckle correlator. Opt Comm 1998;149:355–65.
[6] Kaufmann G. Advances in speckle metrology and related techniques. John Wiley and Sons; 2011.
[7] Uno K, Uozumi J, Asakura T. Speckle clustering in diffraction patterns of random objects under ring-slit illumination. Opt Comm 1995;114:203–10.
[8] Lencina A, Tebaldi M, Vaveliuk P, Bolognini N. Dynamic of speckle clusters formation. Waves Random Complex Medium 2007;17:29–42.
[9] Nye JF, Berry MV. Dislocations in wave trains. Proc R Soc Lond A 1974;336: 165–90.
[10] Jackson JD. Classical Electrodynamics. John Wiley and Sons); 1998.

[11] Allen L, Beijersbergen MW, Spreeuw RJC, Woerdman JP. Orbital angular momentum of light and the transformation of Laguerre-Gaussian laser modes. Phys Rev A 1992;45:8185–9.
[12] Vasnetsov M, Staliunas K. Optical Vortices, 228, Horizons of World Physics—Nova Science 1999.
[13] Marrucci L, Manzo C, Paparo D. Optical spin-to-orbital angular momentum conversion in inhomogeneous anisotropic media. Phys Rev Lett 2006;96: 163905.
[14] Baranova NB, Zel'dovich VI, Mamaev AV, Pilipetskii NF, Shkunov VV. Dislocations of the wavefront of a speckle-inhomogeneous field (theory and experiment). JETP Letters 1981;33:195–9.
[15] Freund I, Shvartsman N, Freilikher V. Optical dislocation networks in highly random media. Opt Comm 1993;101:247–64.
[16] Rozas D, Law CT, Swartzlander Jr. GA. Propagation dynamics of optical vortices. J Opt Soc Am B 1997;14:3054–65.
[17] Molina-Terriza G, Wright EM, Torner L. Propagation and control of non-canonical optical vortices. Opt Lett 2001;26:163–5.
[18] Wang W, Hanson SG, Miyamoto Y, Takeda M. Experimental investigation of local properties and statistics of optical vortices in random wave fields. Phys Rev Lett 2005;94:103902.
[19] Freund I. Optical vortices in Gaussian random wave fields: statistical probability densities. J Opt Soc Am A 1994;11:1644–52.
[20] Dennis MR. Local phase structure of wave dislocation lines: twist and twirl. J Opt A 2004;6:202–8.
[21] Yu Okulov A. Angular momentum of photons and phase conjugation. J Phys B: At Mol Opt Phys 2008;41:7–13.
[22] Yu Okulov A. Twisted speckle entities inside wavefront reversal mirrors. Phys Rev A 2009;80:013837.
[23] Curtis JE, Koss BA, Grier DG. Dynamic holographic optical tweezers. Opt Comm 2002;207:169–75.
[24] Boiron D, Mennerat-Robilliard C, Fournier JM, Guidoni L, Salomon C, Grynberg G. Trapping and cooling cesium atoms in a speckle field. Eur Phys J D 1999; 7:373–7.
[25] Grynberg G, Horak P, Mennerat-Robilliard C. Spatial diffusion of atoms cooled in a speckle field. Europhys Lett 2000;49:424–30.
[26] Shvedov Vladlen G, Rode Andrei V, Izdebskaya Yana V, Desyatnikov Anton S, Krolikowski Wieslaw, Kivshar Yuri S. Selective trapping of multiple particles by volume speckle field. Opt Exp 2010;18:3137–42.
[27] Staforelli JP, Brito JM, Vera E, Solano P, Lencina A. A clustered speckle approach to optical trapping. Opt Comm 2010;283:4722–7.
[28] Shvedov VG, Rode AV, Izdebskaya YV, Desyatnikov AS, Krolikowski W, Kivshar. YS. Selective trapping of multiple particles by volume speckle field. Opt Exp 2010;18:3137–42.
[29] Yeh P. Introduction to Photorefractive Nonlinear Optics. John Wiley and Sons; 1993.
[30] Huignard JP, Gunter P. Photorefractive materials and their applications. II. Springer Verlag; 1989.
[31] Gómez JA, Lorduy G. H, Salazar Ángel. Improvement of the dynamic range of a fiber specklegram sensor based on volume speckle recording in photorefractive materials. Opt Las Eng 2011;49:473–80.
[32] Gómez JA, LorduyG. H, Salazar Ángel. Influence of the volume speckle on fiber specklegram sensors based on four-wave mixing in photorefractive materials. Opt Comm 2011;284:1008–14.
[33] Marrakchi Jr. A, Tanguay. J, Yu D. Psaltis., Incoherent to coherent optical converter. Opt Eng 1985;24:124–31.
[34] Höller F, Tiziani H. A spatial light modulator using BSO crystals. Opt Comm 1986;58:20–4.
[35] Lasprilla MC, Agra Amorim A, Tebaldi M, Bolognini N. Self-imaging through incoherent to coherent conversion. Opt Eng 1996;35:1440–5.
[36] Frejlich J. Photorefractive Materials, Fundamental Concepts, Holographic recording and Materials Characterization. John Wiley and Sons; 2007.
[37] Tebaldi M, Lasprilla MC, Bolognini N. Analysis of birefringence encoded images. Optik 1999;110:127–36.
[38] Mallick S, Rouède D. Influence of the polarization direction on the two-beam coupling in photorefractive $Bi_{12}SiO_{20}$: diffusion regime. J Appl Phys B 1987; 43:239–45.
[39] Moharam MG, Gaylord TK, Magnusson R, Young L. Holographic grating formation in photorefractive crystals with arbitrary electron transport length. J Appl Phys 1979;50:5642–51.
[40] Harrison B, Kyle M. Foundations of image science. John Wiley and Sons; 2003.
[41] Collet E. Polarized light: Fundamentals and Applications. Marcel Dekker; 1993.
[42] Schaefer B, Collett E, Smyth R, Barrett D. Measuring the Stores polarization parameters. Am J Phys 2007;**75**:163–8.
[43] Lagarias JC, Reeds JA, Wright MH, Wright PE. Convergence Properties of the Nelder–Mead Simplex Method in Low Dimensions. SIAM J Opt 1998;9: 112–47.
[44] Denisenko VG, Minovich A, Desyatnikov AS, Krolikowski W, Soskin MS, Kivshar YS. Mapping phases of singular scalar light fields. Opt Lett 2008;33: 89–91.